Mixing Simulation of a Viscous Newtonian Liquid in a Twin Sigma Blade Mixer

Robin K. Connelly and Jozef L. Kokini
Dept. of Food Science, Center for Advanced Food Technology, Rutgers University, Cook College, 65 Dudley Rd., New Brunswick, NJ 08901

DOI 10.1002/aic.10960
Published online September 5, 2006 in Wiley InterScience (www.interscience.wiley.com).

The flow of a viscous Newtonian fluid in a twin sigma blade mixer over the course of a blade cycle is simulated using FEM with mesh superposition, and the resulting velocity profiles are used to calculate the paths of material points in order to do an analysis of the distributive mixing and overall efficiency of the mixer over time. Visual inspection of the material-point distribution, as well as mixing measures that include the cluster distribution index, scale of segregation and mean length of stretch showed the overall mixing effectiveness of this mixer, although there was some positions that had better distributive and stretch capability than others. The mean time-averaged efficiency was related to the specific blade positions and found to remain above zero, while its standard deviation was reducing over time, indicating that the majority of the material points were experiencing equivalent levels of stretching over time. © 2006 American Institute of Chemical Engineers *AIChE J,* 52: 3383–3393, 2006

Keywords: computational fluid dynamics (CFD), mixing, finite element method (FEM), mesh superposition. particle tracking

Introduction

A very common mixer used in industry for processing highly viscous, past-like materials, such as bread dough, rubber, chewing gum, printers ink, solid-state fermentations and ceramics is the batch twin z or sigma blade mixer[1]. However, the flow characteristics and mixing ability of this type of mixer have not been studied much due to both the complexity of the materials and the complexity of the mixer and its motion. Experimental studies of the mixing effectiveness and the effect of fluid properties includes the work of Hall and Godfrey[1-3], and Ellis et al.[4], as well as Kawaguchi et al.[5] using tracers, and Prakash and Kokini[6,7,8,9] using laser doppler anemometry (LDA). These experimental techniques have been able to determine flow and distributive mixing patterns, as well as finding indications of the effects of rheology and scaleup on those patterns. Prakash and Kokini[6,7,8,9] were also able to use their results from a twin sigma blade Farinograph to calculate the local shear rate, mixing index (also know as flow number), length of stretch and area stretch, as well as the overall mixing efficiency for a Newtonian and two shear thinning model fluids. The newest approach to study the flow and mixing in these complex mixers is with computational fluid dynamics numerical simulation, which has been done by Jongen[10,11] with a Newtonian fluid and Connelly and Kokini[12] with a Newtonian and two shear thinning fluids. The numerical approach was used to show flow and distributive mixing patterns and faults, as well as to provide an analysis of the effectiveness of the distributive and dispersive mixing and the overall mixing efficiency.

The biggest roadblock to directly applying numerical simulation to modeling the mixing in mixers such as the twin sigma blade mixer has been that the geometry is constantly changing with time. Recently, computational fluid dynamics (CFD) finite element method (FEM) numerical simulation techniques have been developed that greatly simplify the issue of mesh creation

Current address of R. K. Connelly: Depts. of Food Science and Biological Systems Engineering, University of Wisconsin-Madison, 1605 Linden Drive, Madison, WI 53706; rkconnelly@wisc.edu.
Correspondence concerning this article should be addressed to J. L. Kokini at kokini@aesop.rutgers.edu.

in a constantly changing geometry by separately meshing the mixing domains and mixing elements, and then superimposing them at a given position. Avalosse[13] introduced the mesh superposition technique (MST), which involves separately meshing the flow domain and the moving elements, and then superimposing them at set time intervals with a penalty formulation of the governing equations used to impose the velocity of the moving parts. MST was used with particle tracking to calculate in 3-D the velocity profile, distributive mixing efficiency and cluster distribution index in a stirred tank with and without baffles for several Reynolds numbers. Avalosse and Rubin[14] used MST with particle tracking as implemented by Polyflow (Fluent, Inc., Lebanon, NH) to model the flow and mixing in 3-D in a single screw and twin screw extruder. They were able to reproduce to within 3% the pressure and velocity profiles in the single screw extruder calculated using the more familiar rotating reference frame technique, with a Bird-Carreau viscous fluid model for HDPE, when using mini-element velocity/constant pressure elements for the interpolation. Connelly and Kokini[15] used this technique in 2-D with Polyflow to demonstrate the effect of single paddle vs. co-rotating twin paddle mixing on the mixer effectiveness using a viscous Bird-Carreau dough model. They also showed how increasingly shear thinning behavior changes the flow and mixing patterns in a 3-D geometrically accurate representation of a fully filled twin sigma blade Farinograph mixer in two-blade configurations,[12] in a way that coincided with the LDA results of Prakash and Kokini.[6,7,8,9]

A similar technique introduced by Bertrand and Tanguy[16,17] superimposes the moving-part geometry on the meshed flow domain using Lagrangian multipliers with a velocity constrain. It has been dubbed the virtual finite element method. Results generated using this technique compared favorably with fixed mesh and experimental results of Tanguy et al.,[18,19] and were used to study the mixing efficiency of helical ribbon mixers.[20] Jongen[10,11] used a modification of this technique as implemented by FIDAP (Fluent, Inc., Lebanon, NH) in order to characterize the flow and mixing in simplified 2-D representations of batch mixers commonly used to mix viscous pastes such as dough, which included the double bladed Plastograph and Do-Corder mixers as well as a planetary mixer and an Eberhart spiral mixer. The simulations with viscous Newtonian fluids characterized the flow type using a nonobjective flow parameter based on the invariants of the velocity gradient tensor[21,22] and limited particle tracking. They were able to discern significant differences in the mixing and potential problem spots in the mixers.

The objective of this work is to analyze the mixing of a highly viscous Newtonian fluid in a twin sigma blade mixer using numerical simulation. The mixing of highly viscous fluids is more difficult because it generally takes place only in the laminar regime. It mainly involves the mechanisms of laminar shear, elongational flow and distributive mixing in order to reduce the scale of segregation, while molecular diffusion (which occurs very slowly) and dispersion act to reduce the intensity of segregation.[1,23] Connelly and Kokini[12] use numerical simulation to analyze the flow and mixing at two positions in the twin sigma blade mixer for viscous Newtonian, power-law and cross-fluid models by calculating mappings of the velocity profiles, shear rate and dispersive mixing index. However, in order to get a complete picture of the distributive mixing ability in a mixer, it is necessary to get an indication if all the material in the mixer will be able to distribute throughout the flow area over time and also experience the levels of stretch required for good laminar mixing. This work does this by first extending the numerical simulation of the flow in a twin sigma blade mixer with a viscous Newtonian fluid model by Connelly and Kokini[12] to a complete cycle of the blades positions. The complete Newtonian flow simulation is used to generate particle tracking data over the course of three blade cycles in order to show the distributive mixing patterns. The results of the particle tracking are then used to do an analysis of the distributive mixing and overall efficiency of the mixer over time.

Materials and Methods

Problem description and simulation methodology

The Farinograph (C.W. Brabender Instruments, Inc., S. Hackensack, NJ) is the model for the sigma blade mixer simulated in this study. It is a low-shear rate, batch mixer commonly used for flour testing with two non-intermeshing, asymmetrical sigma blades that rotate using a 3:2 speed ratio, with the fast (right) blade turning 93 rpm counterclockwise and the slow (left) blade turning 62 rpm clockwise. The mixing bowl, which is 0.0845 m deep and 0.1206 m wide at the top, has a normal working capacity of 650 mL and a total volume of 0.001224 m^3 when filled to the full height of 0.0857 m in the center. In this work, the bowl is considered to be covered and filled to the top with a corn syrup that has a constant Newtonian viscosity of $\eta = 5.4$ Pa · s, as was done experimentally by Prakash and Kokini.[6,7,8,9] The mixer geometry and meshes as used by the FEM simulations are pictured in Figure 1, with the left blade rotated 180° and the right blade rotated 270° from the initial position. The shapes of the sigma blades were provided courtesy of C.W. Brabender Instruments, Inc.

Finite element method (FEM) simulations were carried out as described in Connelly and Kokini[12] using the commercially available software Polyflow 3.9.2 by Fluent, Inc. The mesh superposition technique[12,13,24] was used to account for the movement of the sigma blades. The final bowl mesh was chosen after a preliminary study with the corn syrup fluid model at the initial blade position that examined the problem size, solution time and convergence for a series of bowl meshes containing from 13,872 to 62,034 elements. The final bowl mesh was designed to be coarse in the overfill region and refined near the moving blades, while the blade meshes were designed to have enough refinement to capture the complex shape. Elements were strategically placed in the bowl such that there are two elements between the blade edges and the wall, with the blade edges always falling on an element edge, thus minimizing particles bleeding into the fast moving blade edges during particle tracking with mesh superposition. Particle bleeding is a result of the fact that the paddle surface is determined only to within a mesh element of the actual surface when using mesh superposition. What in one position would be considered just outside the blade surface, in another position can be found to be just inside, thus trapping the material point inside the blade. By creating a flow domain mesh that allows the blade edge to always lie exactly on the edge of a mesh element, the shape is properly maintained in all positions and no particles will be captured by that surface of the blade,

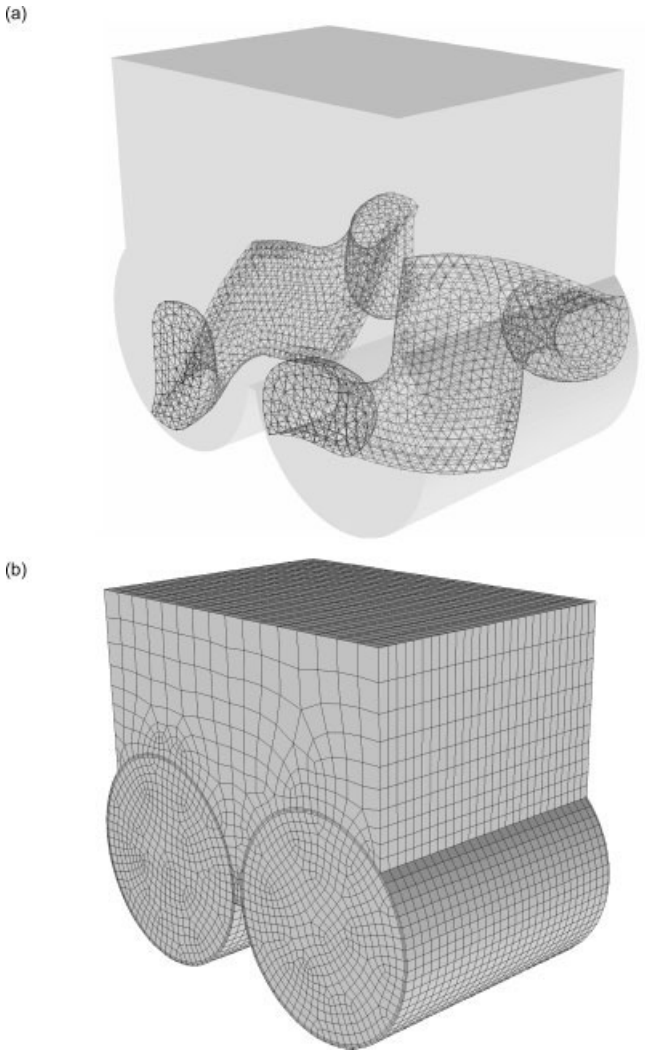

Figure 1. Meshes for the Farinograph (a) blades, and (b) bowl (41860 hexahedral elements).

The slow left blade (62 rpm clockwise) has 6232 tetrahedral elements, and the fast right blade (93 rpm counterclockwise) has 6166 tetrahedral elements.

although particle bleeding on other surfaces of the blades is still possible.

An unsteady-state, time-marching scheme was used in order to do a full mixing analysis including particle tracking. Because the blades turn at different speeds, two revolutions of the slow blades and three revolutions of the fast blade are required before there is repetition of the blade positions for a total cycle time of 1.9355 s. With the bowl mesh used in this study, the optimal time interval between positions is 0.00896 s, such that only one boundary layer element is crossed per position of the fast blade for a total of 216 time steps, giving 3.333° between positions for the slow blade, and 5° between positions for the fast blade. However, due to software and run time constraints, a more practical time interval of 0.02688 s for a total of 72 positions has been chosen. This gives a 10° interval between positions of the slow blade and a 15° interval between positions of the fast blade. Some results during the first revolution of the slow blade have also been generated using a 0.01344 s time interval between positions to check for error due to the size of the time step.

The time marching flow simulation results are then used to generate particle tracking data for 10,000 massless material points initially randomly distributed throughout the flow domain, and three sets of 1,000 massless material points initially randomly distributed in a 1 cm^3 box. The positions of the three boxes are shown in Figure 2, and are labeled B1, which is located between the blades ($-0.005 < x < 0.005$; $0.03725 < y < 0.04725$; $-0.03675625 < z < -0.02675625$); B2, which is near the right blade ($0.04985 < x < 0.05985$; $0.0495 < y < 0.0595$; $-0.005 < z < 0.005$); and B3, which is near the left blade ($-0.05985 < x < -0.04985$; $0.0645 < y < 0.0745$; $-0.005 < z < 0.005$). The positions are given in meters using an origin centered between the two blades' axes of rotation, which is 0.0818 m from the top on the back face with positive x pointing left toward the fast blade, positive z pointing down and positive y pointing toward the front of the mixer. B1 is centered between the front and back of the mixer and slightly higher than the horizontal plane through the center of both blades, in the area shown in the simulations in Connelly and Kokini[12] to have consistently high-shear rates and mixing index values, that will lead to highly effective distributive and dispersive mixing. The positions of clusters B2 and B3 are initially outside the interblade region, but near one of the blades. They are centered on the horizontal plane that goes through the center of rotation of both blades as shown in the front views in Figure 2, with B2 closer to the center of the mixer near the fast right blade and B3 closer to the front of the mixer near the slow left blade as shown in the top views in Figure 2.

The trajectories of the massless material points or particles are calculated by the time integration of the equation $\dot{\mathbf{x}} = \mathbf{v}$ using a fourth-order explicit Runge-Kutta scheme within an element, with local rather than global coordinates. The time step is sized such that the final position in crossing an element is always on the element boundary, so that the element coordinates may be transformed to the local coordinates of the next element to be crossed before continuing the integration. The sum of the steps when transformed to global coordinates gives the successive positions of the particles in real space.[25,26,27] The

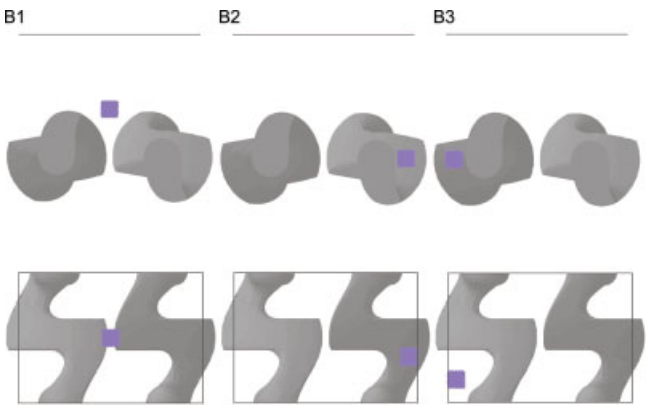

Figure 2. Initial 3-D positions of clusters of 1000 noncohesive material points.

[Color figure can be viewed in the online issue, which is available at www.interscience.wiley.com.]

default of an average of three steps to cross an element has been chosen for the time integration, with the particle positions and kinematic parameters recorded exactly at the same time interval as that used between blade positions (0.026882 s).

The ability of the mixer to distribute the three clusters of 1,000 massless material points is similar to the situation where a minor ingredient needs to be distributed throughout the fluid mass from an initially concentrated addition point. A statistical approach to determining how well this is accomplished makes use of the discrete pair-wise correlation function to compare the distances between each possible pair of points in an optimal random distribution to those across a series of times for a given cluster. The discrete pair-wise correlation function is defined as

$$f(r) = \frac{2}{N(N-1)} \sum_i \delta(\mathbf{r}_i' + \mathbf{r})\delta(\mathbf{r}_i') \approx c(r)\Delta r$$

where $\delta(r) = 1$ if a particle is present, and 0 if absent in the shell of radius $r \pm \Delta r/2$ around the point i located at $\mathbf{r}_i'$, N is the number of particles, and c(r) is the coefficient of the probability density function. The area under the curve of c(r) is a constant, independent of the shape of the distribution, therefore

$$\sum_{r=0}^{r=r_{\max}} c(r)\Delta r = 1$$

where $r_{\max}$ is the largest dimension of the system such that $c(r > r_{\max}) = 0$. An index of the difference between an actual distribution at any given time, and the ideal case defined using the optimal random distribution is then given as[28,29,30]

$$\varepsilon = \frac{\int_0^\infty [c(r) - c(r)_{\text{ideal}}]^2 dr}{\int_0^\infty [c(r)_{\text{ideal}}]^2 dr}.$$

This pair-wise correlation function index (ε), which has recently been described as the "cluster distribution index",[30] is the normalized deviation of the density of probability function for the cluster at a given time from the density of probability function of the optimal random distribution. As the distribution of the initially concentrated cluster of massless material points becomes more like the optimal random distribution over time, ε decreases. While this parameter is independent of the size of the flow domain, it is very dependent on the initial position and size of the cluster. It is also dependent on the number of particles in the cluster, since it cannot measure deviation of the distribution for distances less than mean distance between neighboring particles in the optimal case.

In order to evaluate the overall distributive mixing ability of the mixer, particles randomly distributed throughout the flow domain with an initial y coordinate > 0 are arbitrarily assigned a concentration value of $c = 1$, while the rest of the particles are arbitrarily given a concentration of zero. Then the positions of the particles at any given time are used to calculate the value of the scale of segregation, which is defined as [23,32,33,34]

$$L_s = \int_0^\zeta R(|r|)d|r|$$

where

$$R(|r|) = \frac{\sum_{j=1}^M (c_j' - \bar{c}) \cdot (c_j'' - \bar{c})}{MS^2}.$$

$R(|r|)$ is the Eulerian coefficient of correlation between concentrations of pairs of points in the mixer separated by $|r|$ where $R(0) = 1$ for points having the same correlation, and $R(\zeta) = 0$ at large $|r|$, where there is no correlation. The number of pairs is $M = N(N-1)/2$, where N is the number of points, and S^2 is the sample variance. The concentration of the points in the jth pair is c_j' and c_j'', while $\bar{c}$ is the average concentration. [23,32,33,34] The minimum value occurs when the initially segregated particles become randomly distributed. It is a function of the number of particles tracked and the size of the flow domain. Calculation of the scale of segregation is done at each recorded time step in order to track the evolution of this parameter over time. If there are dead spots or faults in the flow that create areas of the mixer where parts of the initially segregated material cannot reach, this parameter will not be able to reduce to the minimum value. However, the segregation scale is a global average value that cannot pinpoint the exact location, size or number of local flow defects.

Given the motion $\mathbf{x} = \boldsymbol{\chi}(\mathbf{X},t)$, where $\mathbf{X} = \boldsymbol{\chi}(\mathbf{X},0)$ of the particles, the length of stretch of the infinitely small material line associated with each material point is defined as $\lambda = |\mathbf{dx}|/|\mathbf{dX}|$ where the arithmetic mean $\bar{\lambda}$, has been shown to be directly related to the geometric mean striation thickness and is a measure of the growth of the interfacial area.[35,36,37] An exponential increase in the length of stretch over time is a necessary requirement for effective mixing.[22] The local or instantaneous efficiency of mixing for isochoric flows is defined as[38,39]

$$e_\lambda = \frac{\dot{\lambda}/\lambda}{(\mathbf{D}:\mathbf{D})^{1/2}} = \frac{-\mathbf{D}:\hat{\mathbf{m}}\hat{\mathbf{m}}}{(\mathbf{D}:\mathbf{D})^{1/2}} = \frac{D \ln \lambda / Dt}{(\mathbf{D}:\mathbf{D})^{1/2}},$$

where $\mathbf{D}$ is the rate of strain tensor, $\hat{\mathbf{m}}$ is the current orientation unit vector, and $(\mathbf{D}:\mathbf{D})^{1/2}$ is the limit of $-\mathbf{D}:\hat{\mathbf{m}}\hat{\mathbf{m}}$ according to Cauchy-Schwarz's inequality. The efficiency can be thought of as the fraction of the energy dissipated locally that is used to stretch a fluid element at a given instant in a purely viscous fluid[22] and falls in the range $\{-1,1\}$. A value of -1 would indicate that all the energy dissipated was used to shorten the length of the material line, in effect completely unmixing it, while a value of 1 indicates that all the energy dissipated was used to stretch the material line. The time-averaged efficiency is defined as[22]

$$\langle e_\lambda \rangle = \frac{1}{t} \int_0^t e_\lambda dt.$$

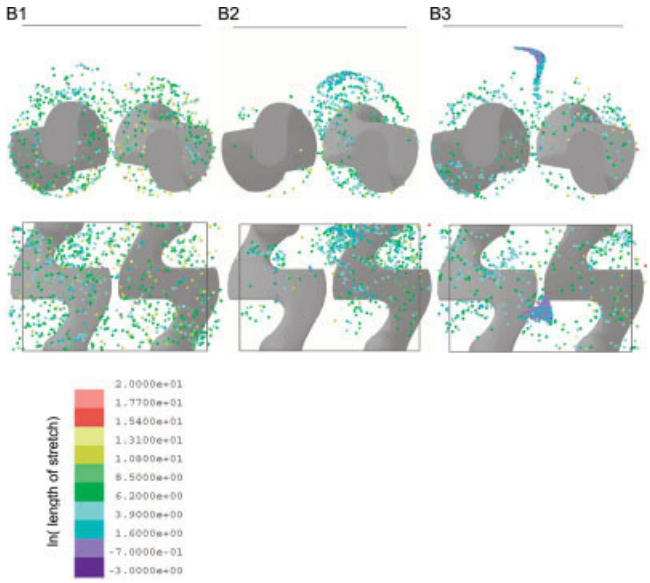

Figure 3. 3-D positions of 1,000 initially clustered material points after three blade cycles (6 revolutions of slow left blade, and 9 revolutions of fast right blade).

[Color figure can be viewed in the online issue, which is available at www.interscience.wiley.com.]

Typical behavior of the time-averaged mixing efficiency ranges from the decay of the efficiency with time as t^{-1} for flows with no reorientation, such as the simple shearing flows, to flows with some periodic reorientation, but still decaying on average with time as t^{-1}, to the optimum case for mixing, which is flows with strong reorientation that have an average constant value of the efficiency.[22]

Results and Discussion

Distributive mixing of selected clusters

The effect of the initial position of the clusters on the distributive mixing is striking as can bee seen in Figure 3. During the first blade cycle, the B1 cluster initially between the blades has been split and stretched both radially around the blades, and axially toward both the front and the back. After three blade cycles, the material points in B1 appear to be randomly distributed in the flow area swept by the blades, although none of the points have approached the low-flow region away from the blades near the top of the mixer.

During the first blade cycle, the B2 cluster located near the center of the fast right blade has moved toward the back of the mixer and stretched radially about one time around the right blade. Even after three cycles of the blades, its material points remain mainly in the left rear quadrant of the mixer as seen in Figure 3, with just a limited amount of material escaping into the rest of the mixer. Within that quadrant, the material seems to have become well distributed.

The B3 cluster has moved up above the blades toward the geometric center of the mixer and remains an elongated cluster, with a tail that is slowly getting sucked into the center of the mixing flow at about the same position as B1 was initially. The material from the clump that enters that position quickly distributes into the flow in a manner similar to cluster B1. After three cycles, Figure 3 shows that most of cluster B3 has been pulled into the highly effective center zone and distributed throughout the area of the mixer, except for a small section of the clump that is still moving very slowly into the effective mixing zone.

The material points in Figure 3 are colored by the natural log of the length of stretch experienced by an initially randomly oriented infinitesimal line located on the material point, where the length of stretch is equal to the ratio of the current length over the original length of the infinitesimal line, and the scale ranges from dark blue indicating little stretch, or a reduction in length to red indicating the highest stretch values. As the length of stretch for the points is examined locally, it is obvious that very little stretching of the cluster B3 material points takes place until they are pulled into the highly effective center zone. Also, a general increase in the length of stretch of cluster B1 and B2 is seen of around the same magnitude. However, in both cases even after three cycles, there are points that have not stretched or even have become compressed. Those points do not appear to have become attached to the walls or stuck in the upper low-flow region, but rather seem to be in the grip of flow regions where the material is moving, but not deforming. The points are generally located in the areas between the wide central section of the blades, and the curved sections of the blades that sweep the front and back of the bowl, which is also about the location where the cluster B3 was initially located. When compared with the velocity vectors, mixing index and shear rates mapped in Connelly and Kokini,[12] it can be seen that these points are in areas that have been shown to have poorer mixing potential.

The cluster distribution index (ε) is shown for these clusters over three blade cycles in Figure 4. The quick distribution of B1 is shown by the quick drop in the value of ε, followed by a slower, but still evident continued lowering as the material points become ever more random in the less effective regions of the mixer. The movement with little deformation followed by some compression of B3 is also seen in the ε value, with the

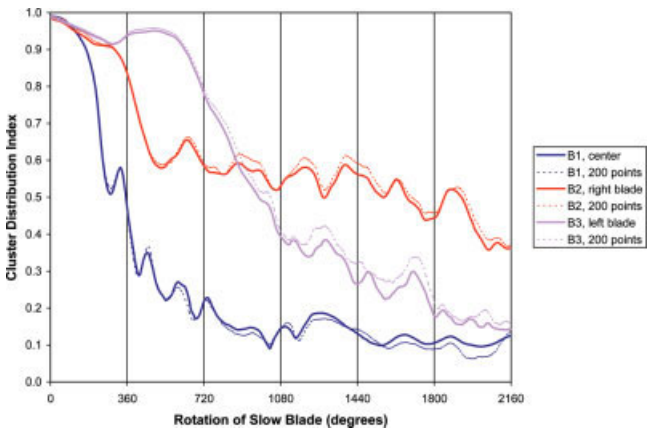

Figure 4. Evolution of the cluster distribution index of three material point clusters over 3 cycles of the blades (6 revolutions of slow (left) blade/9 revolutions of fast (right) blade).

[Color figure can be viewed in the online issue, which is available at www.interscience.wiley.com.]

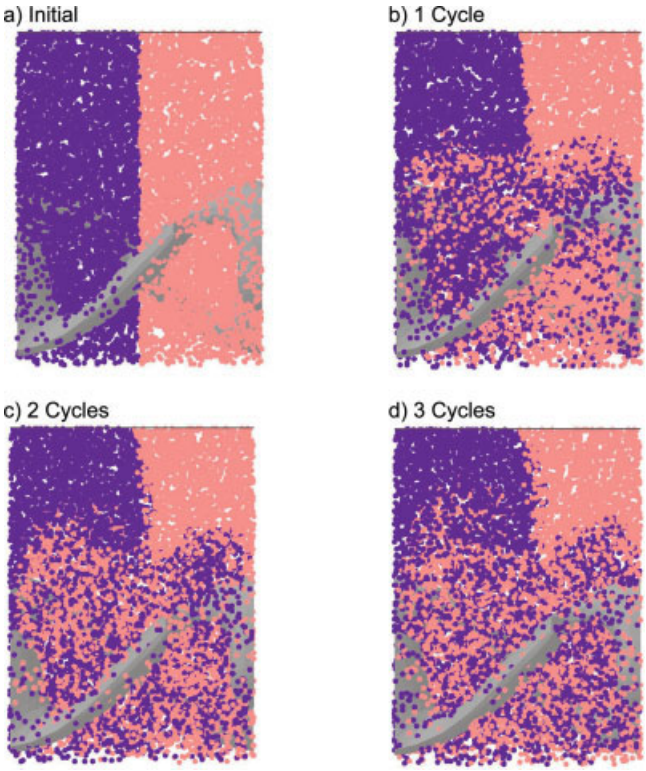

Figure 5. 3-D positions of 10,000 initially randomly distributed material points with concentrations of 1 (red/light grey) in the back, and 0 (blue/dark grey) in the front viewed from the right-side.

[Color figure can be viewed in the online issue, which is available at www.interscience.wiley.com.]

quick distribution of the tail as it is slowly pulled into the highly effective zone causing the steady decrease seen starting with the second blade cycle until it is nearly equivalent with B1 by the end of the third blade cycle. The inability of cluster B2 to leave the right rear quadrant is also evident by the quick drop of the ε as the points distribute throughout that quadrant, followed by an almost steady value that is substantially higher than the value reached by B1 and B3 clusters, which have distributed nearly randomly over the entire region swept by the blades. The nonzero value at which ε is leveling off is due to the much slower ability of this mixer to move material in and out of the region above the area swept by the blades, although B3 did enter the edge of this region, which is why it was so slow to stretch and distribute. However, this would not be a problem in the normal operation of this mixer, since it is generally not filled there.

In order to indicate the extent of the error in using a limited number of data points, the ε value was calculated using a random subset of 200 of the 1,000 points and compared to that calculated with the full set of points. The overall RMS difference between the cluster distribution indexes calculated using all 1,000 material points and only a subset of 200 randomly chosen material points was 1.55% of the initial ε value using 1,000 points for B1, 1.57% for B2 and 2.6% for B3 over three complete cycles, with the error increasing with increasing number of blade cycles. Note that the error measured here does not consider the likely substantial error between the simulation and an actual experiment that would be due to the rather large time steps in the blade position used, but does illustrate that the error would be increasingly important over time. Fortunately, during the initial stages of the mixing, even the 200 material point cluster captures the overall behavior within the capability of this measure.

Distributive Mixing Between Halves of the Farinograph

In order to investigate the overall distributive ability of the mixer, 10,000 material points were initially randomly distributed throughout the entire 3-D flow domain not containing the blades. Then the points were initially assigned a concentration value of 1 (red/light gray) or 0 (blue/dark gray) in one of two ways: the points with $0 \leq y < 4.225$ in the front half of the mixer were assigned a concentration value of 0 and all others in the back half of the mixer a value of 1, as shown in Figure 5a, or the points with $x > 0$ on the right-side of the mixer were assigned a concentration value of 0 and all others on the left-side were assigned a value of 1, as shown in Figure 6a. The positions of the points were tracked as the blades moved. The results after 1, 2 and 3 cycles of the blades are shown in Figures 5b–d, and 6b–d.

In the 3-D view in Figure 5, it can be seen that the material quickly distributes between the front and back of the mixer in the area swept by the blades, while the material points in the area near the top of the mixer away from the blades show very little distributive mixing with the interface between the two concentrations remaining intact and almost unchanged except for a tendency to lean toward the back of the mixer after three cycles of the blades. After three cycles, the entire area swept by the blades appears to be randomly distributed within the level

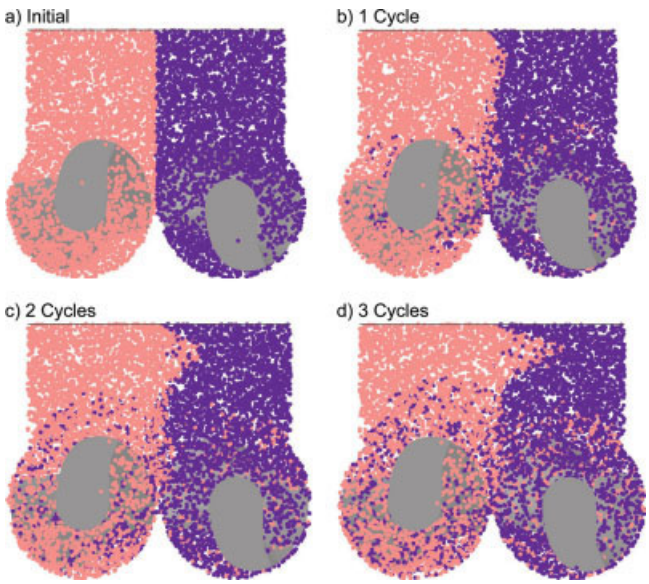

Figure 6. 3-D positions of 10,000 initially randomly distributed material points with concentrations of 1 (red/light gray) on the left, and 0 (blue/dark gray) on the right, viewed from the front.

[Color figure can be viewed in the online issue, which is available at www.interscience.wiley.com.]

of resolution provided by 10,000 material points. The area just above that swept by the blades shows evidence of a slow flow pattern that is pulling material up from the area swept by the blades away from the interface, and then down into the area swept by the blades at the interface. This would explain why the interface is staying so intact. There also appears to be a tendency of the fast blade to pull the material toward the back of the mixer. Both of these effects were also noted in the behavior of the clusters in the previous section.

The exchange between the left and right sides of the mixer shown in 3-D front view of the mixer in Figure 6 is slower than the exchange of material between the front and back shown in Figure 5, but still appears very effective. Material near the front and back walls remains completely segregated after three cycles, but the depth of the segregated area is thinning. A slow circulation pattern is evident in the area above that swept by the blades that pulls material up above the slow blade, over toward the right wall, and then down toward the fast blade, likely caused by the differential in the blade speeds. The area swept by the blades in the center of the mixer is difficult to see, but it appears that material is pulled in from the opposite side near the center and below the slow blade or above the fast blade, and then is distributed toward the front and back by the mechanisms described above. This is likely caused by the squeezing action of the blades, with the edges passing close to each other followed by a pulling behind that section. Additional pumping action is likely provided by the speed differential between the blades.

The distributive mixing action shown in Figures 3, 5 and 6 can be summarized in general as the fast blade pulling material down from the top and over from the slow blade, and then pushing it under the slow blade near the bottom where the cylindrical chambers divide. The slow blade pushes the material up toward the top and over to the fast blade. While material is in the area swept by a blade, it is also being quickly distributed from the center toward the front and back walls of the mixer, and then pushed up above the blades and slowly back toward the center, with a slow tendency to move more toward the back of the mixer above or near the fast blade. The evidence indicates that the speed differential improves the ability of this mixer to distribute material that is above the area swept by the blades, because the greater pumping action of the fast blade requires more material than can be delivered by the slow blade, thus, promoting the left to right flow pattern near the top evident in Figure 6.

The segregation scale is shown for these two initial concentration distributions in Figure 7. The difference in the initial values of the segregation scale for the two initial concentration distributions is due to the variation in the shape of the two volumes. Since the overall volumes are identical, the left/right segregation is found to be initially mathematically larger than the front/back segregation and, therefore, has more distribution needing to take place. The change in the segregation scale for the two initial concentration distributions is similar after three cycles of the blades (2.05 for left/right and 2.28 for front/back). However, the trends of the two lines are much different, with the front/back distribution dropping off quickly and then leveling off, while the left/right distribution drops off more slowly but steadily. From the observed slope of the lines at the end of three cycles, it is expected that the left/right distribution would continue to drop off, while the front/back distribution would

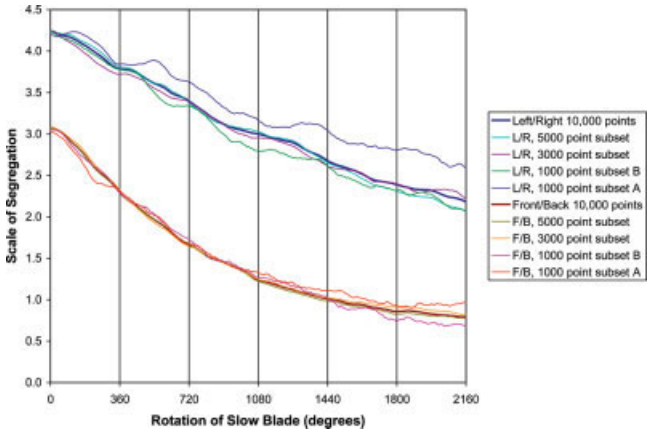

Figure 7. Segregation scale in cm for material initially segregated between the front and back, or the left and the right sides of the mixer over three cycles of the blades.

[Color figure can be viewed in the online issue, which is available at www.interscience.wiley.com.]

change much more slowly, leading in the end to a potentially better distribution in a shorter time by the initially left/right segregated distribution of concentrations. This is in agreement with the mixing patterns observed earlier.

The RMS difference between the segregation scale calculated over three blade cycles with the left/right distribution, using the entire set of 10,000 material points and two randomly generated subsets of 1,000 material points, is 6.6% of the initial value of the segregation scale calculated with 10,000 points for subset A, with the difference increasing steadily with increasing revolutions, and 2.5% with subset B, with the difference having reached a maximum of 4.9% and then slowly decreasing. Based on the segregation scale plots of these subsets shown in Figure 7, these differences likely indicate that subset A is over-representing the slow mixing areas of the flow, while subset B is under-representing the slow mixing areas in the left/right distribution. Independent subsets of 3,000 and 5,000 points have less difference with the 5000 point subset staying within 2.8% of the 10,000 point segregation scale values, and having a RMS error in comparison to initial values calculated with the entire set of 10,000 material points over three blade cycles of less the 1.2% for both the left/right distribution and the front/back distribution, thus indicating that the 10,000 material point segregation scale results are converging on the actual values within the available level of resolution.

Efficiency of Mixing

Figure 8 shows the evolution of the length of stretch of the initially randomly oriented infinitesimal lines associated with all 10,000 of the material points. Because of the large number of points and the difficulty of seeing the exact 3-D position of the points in a 2-D representation, only a few general observations are possible. The material in or very near the moving parts of the mixer experiences stretch, and the distribution of the stretch appears to be relatively randomly scattered around a given blade, although more high-stretch values are found close to the maximum radius of the blades than closer to the blade center of rotation. More high-stretch values are also

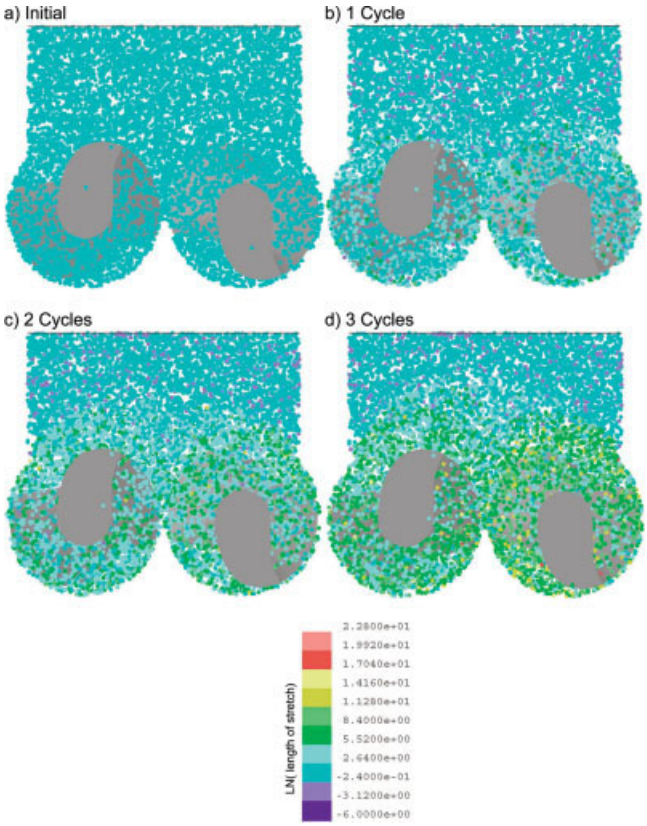

Figure 8. 3-D front views of the positions of 10,000 initially randomly distributed material points colored by the natural log of the length of stretch.

[Color figure can be viewed in the online issue, which is available at www.interscience.wiley.com.]

found around the fast blade than around the slow blade. The position of the higher percentages of highly stretched material coincides with where the blade is moving the fastest and, therefore, covering the most ground and having the highest shear and elongation rates. The fact that high-stretch values can be found outside those high-shear zones is an indication of the effectiveness of the mixing. Moving away from the region swept by the blades, the amount of stretch experienced by the material is reduced until near the top a significant portion of the infinitesimal lines are shorter than their original length after three cycles, indicating that they have been compressed.

The overall length of stretch experienced by the material is indicated by the mean and standard deviation of the natural log of the length of stretch shown in Figure 9a. The log of the mean value is increasing linearly, which indicates the exponential growth necessary for effective mixing.[22] The evolution of the density of probability for the natural log of the length of stretch in Figure 9b shows that over time a large amount of material is steadily increasing its length of stretch. This is likely the material initially in the area swept by the blades. Another initially larger amount of material appears to be almost unstretched, but the amount of that material is steadily decreasing over time. This is likely the much slower moving material in the overfill region above the blades.

For the first 1.5 cycles, the error between the length of stretch results generated by the 10,000 material points and the 4 independent subsets is insignificant, but after that it begins to increase steadily for a maximum of ~4.5% of the current 10,000 point length of stretch value at the end of the third cycle. The RMS %error is 2.85% over the three cycles for 1,000 point subset A, exclusive of the first half turn of the slow blade due to the small size of the length of stretch at that point causing difficulties with the normalization. The difference between 10,000 material point curves generated using 72 time steps per blades cycle and 144 time steps per blade cycle during the first revolution of the slow blade has only a maximum of 1.37% of the 144 time step length of stretch value, and a RMS error of 1.12% even when including the initial values. This error is extremely low when considering the size of the time steps, and that the two simulations used independent, randomly generated sets of material points. However, in order to insure a valid solution over longer time periods than shown here, the number of points needed would need to be increased and the size of the time step decreased due to the logarithmic increase of the error.[22]

The average values of the instantaneous and time-averaged

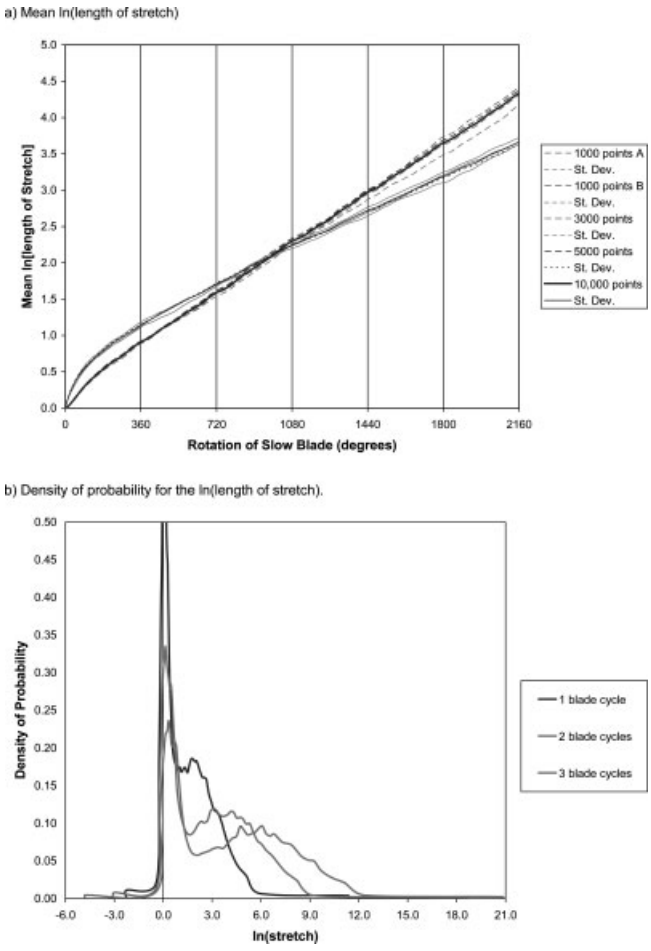

Figure 9. The length of stretch experienced by 10,000 infinitesimal material lines over three cycles of the blades: (a) Mean ln(length of stretch), and (b) density of probability for the ln(length of stretch).

[Color figure can be viewed in the online issue, which is available at www.interscience.wiley.com.]

efficiency over three cycles of the blades are shown in Figures 10 and 11. The instantaneous efficiency shows a definite pattern that repeats over each blade cycle. It is similar to the pattern recorded over time at a single location during mixing of 2% CMC in the Farinograph in Prakash.[6] The 0° position of the blades shown in the particle tracking figures and 360° position of the slow blade are the least efficient in terms of the amount of the energy that is being used to deform rather than displace the material points. In those positions, the flat central sections of both blades are horizontal at the same time and would be impeding the circulation patterns that move material between the left and right sides of the mixer discussed in the previous section. The 0° position of the blades also has the highest standard deviation, indicating that there is a wider or flatter distribution of efficiencies being experienced by the material points at that position of the blades.

The six peaks in the efficiency curves per blade cycle correspond to when the flattened central portion of the fast blade is vertical, and their shapes follow a distinct pattern. The 2nd and 5th peaks correspond to when the flattened central section of the slow blade is horizontal, but only the 2nd peak has the lower magnitude that would be expected due to the inefficiency of the horizontal position of the slow blade. The slow blade is in an identical position for both of these peaks, but the fast blade is flipped 180° between them with a position rotated 90° from the position shown in the particle tracking figures at peak 5. The other two times that the fast blade is in the 90° position is at peak 1 and peak 3, which generally show the highest overall values of the mean instantaneous efficiency. Therefore, the conclusion is that the 90° position of the fast blade is the most efficient, possibly due to enhancement of the front to back slow mixing pattern discussed earlier.

The difference in the mean-instantaneous efficiency generated by material point subsets and 10,000 material points varies in both the positive and negative directions and does not appear to be cumulative error. Use of 1,000 points is clearly insufficient, because the pattern over a cycle of the blades is much less apparent and the instantaneous efficiency values, especially at the peaks and valleys of the curve, vary as much as

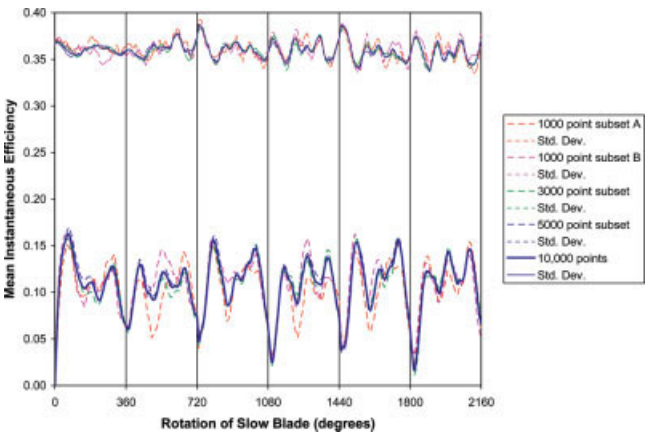

Figure 10. Mean instantaneous efficiency of the mixing experienced by 10,000 infinitesimal material lines over three cycles of the blades.

[Color figure can be viewed in the online issue, which is available at www.interscience.wiley.com.]

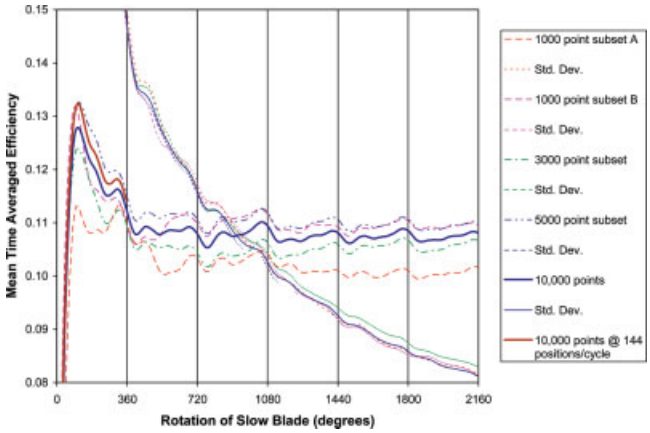

Figure 11. Mean time-averaged efficiency of the mixing experienced by 10,000 infinitesimal material lines over three cycles of the blades.

[Color figure can be viewed in the online issue, which is available at www.interscience.wiley.com.]

45% from the 10,000 point values. However, the 10,000 point curve is much smoother and a definite pattern based on the blade position is apparent, indicating that 10,000 points allows correct conclusions to be drawn. Use of a smaller time step generated a maximum difference of 5.2% of the 10,000 point value and a RMS %difference of 2.25% after 1 revolution of the slow blade. However, the difference between the results using the two different time steps varied in a similar fashion to that for smaller material point subsets, and, therefore, is due at least in part to the difference between the randomly generated initial positions of the points. It is expected that use of more points to calculate the instantaneous efficiency would further smooth the curve and decrease variability in shape of the curve between cycles, but not change the conclusions that have been drawn.

The evolution of the mean of the time averaged efficiency is shown in Figure 11. Major differences are seen during the initial cycle of the blades for each subset of material points as well as between the simulation results generated with two different time steps. However, while it is recommended to calculate the time averaged efficiency with a larger set of material point data in order to assure the validity of conclusions, the smoothness and consistent pattern seen in the 5,000 and 10,000 material point curves indicates that they are providing an adequate solution. These curves show the typical quick rise in the time-averaged efficiency as the material initially begins to move, followed by a fast drop-off as the material points in rotational patterns or in dead zones fail to maintain a logarithmic increase in the length of stretch. Then, the curve levels-off at a value above zero, which is a requirement for an effective mixer. Looking more closely at the mean time-average efficiency curves, it can be seen that after the first cycle there is a pattern to the curve that is reflective of the behavior seen in instantaneous efficiency curve that is used to calculate the time-averaged efficiency. After each revolution of the slow blade, where the low points in the instantaneous efficiency curves occur, there is a drop in the time-averaged efficiency followed by a gradual rise with small local peaks corresponding to peaks 1 and 3 during the first revolution of the

slow blade in a cycle, and peaks 4, 5 and 6 during the second revolution of the slow blade in a cycle. The effectiveness of this mixer is further shown by the continuous decrease of the standard deviation with increasing revolutions of the blade shown in Figure 11, indicating that the majority of the material points are experiencing stretch within a narrowing range and, therefore, are being effectively moved into the high-shear/high elongation regions of the flow domain.

Conclusions

Numerical simulation of the flow and mixing of a viscous Newtonian fluid in a fully-filled batch Farinograph mixer, using the mesh superposition technique and particle tracking, has been used to show the flow and mixing patterns that bring about the high-effectiveness of the twin sigma bladed C.W. Brabender Farinograph. We have been able to show that the differential in the blade speeds allows an exchange of material between the blades to occur with a circulation pattern of material moving up toward the top and over toward the fast blade from the slow blade, while the fast blade pushed material toward the slow blade near the bottom of the mixer. Another slower mixing pattern of material around the blades moving from the center toward the walls, and then up toward the top and back down in the center of the mixer is also observed. The zone in the center of the mixer between the two blades is shown to have excellent distributive mixing ability with high-shear rates and mixing index values, as well as fast distribution throughout both sides of the lower section of the mixer of material point clusters that travel through that region. In contrast, the area away from the region swept by the blades that is generally not filled during normal use of this mixer demonstrates very slow mixing that is made worse by the presence of shear thinning.[12] The mean length of stretch calculated for material points in the Newtonian fluid increased exponentially, indicating effective mixing of the majority of material points. In the area swept by the blades, the highest values of the length of stretch are generally located near the blade edges or in the area swept by the blade edges, but high points are also found outside these zones in a more random position. The instantaneous efficiency gives a picture of which blade positions are the most and least effective at applying energy to stretch rather than displace material points. The least effective positions are when the flattened central sections of both blades are horizontal, while the most effective mixing occurs when the flattened section of the fast blade is vertical. The mean time-averaged efficiency stays above zero, while its standard deviation reduces over time, indicating that the majority of the points are experiencing equivalent levels of stretching over time.

These mixing analysis results demonstrate the mixing effectiveness of the twin-sigma bladed C.W. Brabender Farinograph, and also show how CFD numerical simulation with particle tracking can provide process designers a way to examine the flow and mixing in a complex mixer. The improvement in computational capabilities of both the hardware and software seen during the course of this work is continuing and should ultimately lead to routine use of computation methods as a tool for mixer design and selection. Numerical simulation offers an alternative way to bring together and test the interactions of the models that explain the mixing process. The understanding gained will then allow the design of mixing systems that produce consistent final products with the desired structural and functional characteristics that result from effective mixing.

Acknowledgment

This is publication No. D10544-4-05 of the New Jersey Agricultural Experiment Station, supported by the National Research Initiative of the USDA Cooperative State Research, Education and Extension Service grant number 2001-35503-10127, and the Center for Advanced Food Technology (CAFT). The Center for Advanced Food Technology is a New Jersey Commission on Science and Technology Center.

Literature Cited

1. Harnby N, Edwards MF, Nienow AW, eds. *Mixing in the Process Industries.* 2nd ed. Oxford, G.B.: Butterworth/Heinemann; 1992.
2. Hall KR, Godfrey JC. The mixing rates of highly viscous Newtonian and non-Newtonian fluids in a laboratory sigma-blade mixer. *Trans Inst Chem Engrs*. 1968;46:205-212.
3. Hall KR, Godfrey JC. The effect of fluid properties and mixer size on the performance of batch mixing machines. In: *Proceedings of the 1st National Conference on Rheology*. May 30-June 1, 1979; Melbourne, Australia; p 77-81.
4. Ellis SP, Gray KR, Biddlestone AJ. Mixing evaluation of a Z-blade mixer developed as a novel solid state bioreactor. *Trans Inst Chem Engrs*. 1994;72(Part C):158-162.
5. Kawaguchi Y, Kaminoyama M, Nishi K, Kamiwano M. Analysis of mixing process for wet particle system in a double blade batch kneader mixer. *J Chem Engr Japan*. 1997;30(3):550-556.
6. Prakash S. *Characterization of Shear Rate Distribution in a Model Mixer Using Laser Doppler Anemometry.* New Brunswick, NJ, Dept. of Food Science, Rutgers University; 1996. PhD. Thesis.
7. Prakash S, Karwe M, Kokini JL. Measurement of velocity distribution in the Brabender farinograph as a model mixer, using Laser-doppler anemometry. *J Food Proc Eng*. 1999;22:435-454.
8. Prakash S, Kokini JL. Determination of mixing efficiency in a model food mixer. *Adv Poly Tech*. 1999;18(3):208-224.
9. Prakash S, Kokini JL. Estimation and prediction of shear rate distribution as a model mixer. *J Food Engr*. 2000;44:135-148.
10. Jongen T. Characterization of batch mixers using numerical flow simulations. *AIChE J*. 2000;46(11):2140-2150.
11. Jongen TRG, Bruschke MV, Dekker JG. Analysis of dough kneaders using numerical flow simulations. *Cer Chem*. 2003;80(4):383-389.
12. Connelly, R.K. and Kokini, J.L. 3D Numerical Simulation of the Flow of Viscous Newtonian and Shear Thinning Fluids in a Twin Sigma Blade Mixer. *Adv Poly Tech.* 2006;25(3):in press.
13. Avalosse T. Numerical simulation of distributive mixing in 3-D flows. *Macromol Symp*. 1996;12:91-98.
14. Avalosse T, Rubin Y. Analysis of mixing in corotating twin screw extruders through numerical simulation. *Int Poly Proc*. 2000;XV(2): 117-123.
15. Connelly RK, Kokini JL. Examination of the mixing ability of single and twin screw mixers using 2D Finite Element Method simulation with particle tracking. *J Food Engr*. 2006;Pre-publication On-line.
16. Tanguy PA, Bertrand F, Labrie R, Brito-de la Fuente E. Numerical modeling of the mixing of viscoplastic slurries in a twin-blade planetary mixer. *Trans I Chem E*. 1996;74(A):499-504.
17. Bertrand F, Tanguy PA, Thibault F. A three-dimensional fictitious domain method for incompressible fluid flow problems. *Int J Numer Meth Fluids*. 1997;25:719-736.
18. Tanguy PA, Lacroix R, Bertrand F, Choplin L, Brito-de la Fuente E. Finite element analysis of viscous mixing with a helical ribbon-screw impeller. *AIChE J*. 1992;38:939-944.
19. Tanguy PA, Thibault F, Brito-de la Fuente E, Espinosa-Solares T, Tecante A. Mixing performance induced by coaxial flat blade-helical ribbon impellers rotating at different speeds. *Chem Engr Sci*. 1997; 52(11):1733-1741.
20. de la Villéon J, Bertrand F, Tanguy PA, Labrie R, Bousquet J, Lebouvier D. Numerical investigation of mixing efficiency of helical ribbons. *AIChE J*. 1998;44(4):972-977.
21. Astarita G. Objective and generally applicable criteria for flow classification. *J Non-Newt Fluid Mechs*. 1979;6(1):69-76.

22. Ottino JM. *The Kinematics of Mixing: Stretching, Chaos and Transport*. Cambridge University Press; 1989.
23. Tadmor Z, Gogos CG. *Principles of Polymer Processing*, New York: Wiley; 1979.
24. Polyflow. *User's Manual, Version* 3.9. Place del'Universite 16, B-1348 Louvain-la-Neuve, Belgium; 2003.
25. Polyflow. *Mixing User's Manual, Version* 3.9. Place del'Universite 16, B-1348 Louvain-la-Neuve, Belgium; 2003.
26. Debbaut B, Avalosse T, Dooley J, Hughes K. On the development of secondary motions in straight channels induced by the second normal stress difference: experiments and simulations. *J Non-Newt. Fluid Mechs*. 1997;69:255-271.
27. Ishikawa T, Kihara S-I, Funatsu K. 3-D non-isothermal flow field analysis and mixing performance evaluation of kneading blocks in a co-rotating twin screw extruders. *Poly Engr Sci*. 2001;41(5):840-849.
28. Wong TH, Manas-Zloczower I. Two-dimensional dynamic study of the distributive mixing in an internal mixer. *Int Poly Proc*. 1994;9(1): 3-10.
29. Yang H-H, Manas-Zloczower I. Analysis of mixing performance in a VIC mixer. *Int Poly Proc.* 1994;9(4):291-302.
30. Yang H-H, Wong TH, Manas-Zloczower I. Flow field analysis of a banbury mixer. In: Manas-Zloczower I, Tadmor Z, eds. *Mixing and Compounding of Polymers: Theory and Practice.* New York: Carl Hanser Verlag;1994:187-223.
31. Connelly RK, Kokini JL. Analysis of mixing in a model mixer using 2-D numerical simulation of differential viscoelastic fluids with particle tracking. *J Non-Newt Fluid Mech*. 2004;123:1-17.
32. Danckwerts PV. The definition and measurement of some characteristics of mixtures. *Appl Sci Res*. 1952;A3:279-296.
33. Brodkey RS. Fundamentals of turbulent mixing and kinetics. In: Ulbrecht JJ, Patterson GK, ed. *Mixing of Liquids by Mechanical Agitation.* Vol 1. New York: Gordon and Breach Publishers; 1985:29-58.
34. Chella R. Laminar mixing of miscible fluids, In: Manas-Zloczower I, Tadmor Z, eds. *Mixing and Compounding of Polymers: Theory and Practice.* New York: Carl Hanser Verlag;1994:1-25.
35. Alvarez MM, Muzzio FJ, Cerbelli S, Adrover A, Giona M. Self-similar spatiotemporal structure of intermaterial boundaries in chaotic flows. *Phys Rev Let*. 1998;81(16):3395-3398.
36. Muzzio FJ, Alvarez MM, Cerbelli S, Giona M, Adrover A. The intermaterial area density generated by time- and spatially-periodic 2D chaotic flows. *Chem Eng Sci*. 2000;55:1497-1508.
37. Zalc JM, Szalai ES, Alvarez MM, Muzzio FJ. Using CFD to understand chaotic mixing in laminar stirred tanks. *AIChE J*. 2002;48(10): 2124-2134.
38. Ottino JM, Ranz WE, Macosko CW. A lamellar model for analysis of liquid-liquid mixing. *Chem Eng Sci*. 1979;34:877-890.
39. Ottino JM, Ranz WE, Macosko CW. A framework for description of mechanical mixing of fluids. *AIChE J*. 1981;27(4):565-577.

Manuscript received Jun. 21, 2005, and revision received Jun. 23, 2006.